Received: 11 November 2022 | Revised: 5 May 2023 | Accepted: 26 May 2023

DOI: 10.1002/jev2.12348

TECHNICAL NOTE

Label-free discrimination of extracellular vesicles from large lipoproteins

Anna D. Kashkanova[1,2] | **Martin Blessing**[1,2,3] | **Marie Reischke**[1] | **Jan-Ole Baur**[4] | **Andreas S. Baur**[4] | **Vahid Sandoghdar**[1,2,3] | **Jan Van Deun**[4]

[1]Max Planck Institute for the Science of Light, Erlangen, Germany

[2]Max-Planck-Zentrum für Physik und Medizin, Erlangen, Germany

[3]Department of Physics, Friedrich-Alexander-Universität Erlangen-Nürnberg, Erlangen, Germany

[4]Department of Dermatology, Universitätsklinikum Erlangen, Friedrich-Alexander-Universität Erlangen-Nürnberg, Erlangen, Germany

Correspondence
Vahid Sandoghdar, Max Planck Institute for the Science of Light, 91058 Erlangen, Germany.
Emails: Vahid.Sandoghdar@mpl.mpg.de

Jan Van Deun, Department of Dermatology, Universitätsklinikum Erlangen, Friedrich-Alexander-Universität Erlangen-Nürnberg, 91052 Erlangen, Germany.
Email: Jan.VanDeun@uk-erlangen.de

Funding information
Alexander von Humboldt-Stiftung; Max-Planck-Gesellschaft; Bundesministerium für Bildung und Forschung; Christiane Nüsslein-Volhard-Stiftung

Abstract

Extracellular vesicles (EVs) are increasingly gaining interest as biomarkers and therapeutics. Accurate sizing and quantification of EVs remain problematic, given their nanometre size range and small scattering cross-sections. This is compounded by the fact that common EV isolation methods result in co-isolation of particles with comparable features. Especially in blood plasma, similarly-sized lipoproteins outnumber EVs to a great extent. Recently, interferometric nanoparticle tracking analysis (iNTA) was introduced as a particle analysis method that enables determining the size and refractive index of nanoparticles with high sensitivity and precision. In this work, we apply iNTA to differentiate between EVs and lipoproteins, and compare its performance to conventional nanoparticle tracking analysis (NTA). We show that iNTA can accurately quantify EVs in artificial EV-lipoprotein mixtures and in plasma-derived EV samples of varying complexity. Conventional NTA could not report on EV numbers, as it was not able to distinguish EVs from lipoproteins. iNTA has the potential to become a new standard for label-free EV characterization in suspension.

KEYWORDS
concentration, extracellular vesicles, interferometric scattering, lipoproteins, plasma, refractive index, size

1 | INTRODUCTION

Pathological conditions can lead to a dysregulation of the circulating extracellular vesicle (EV) population, including in number and size. While this makes EVs an interesting target for biomarker studies on liquid biopsies, accurate sizing and enumeration of purified EV samples is typically hampered by the presence of co-isolated particles with similar properties as EVs. Lipoproteins (LPs) are a main source of contamination when considering blood plasma. Intermediate-, very-low- and ultra-low-density lipoproteins (IDLs, VLDLs and ULDLs/chylomicrons) are of particular concern, as they outnumber EVs by several orders of magnitude and have an overlapping size range (30–1000 nm, therefore these will be designated in this paper as 'large LPs') (Simonsen, 2017). Furthermore, their concentration in plasma varies with prandial status. Standard EV isolation methods such as differential ultracentrifugation or size-exclusion chromatography fail to remove a large percentage of large LPs (Brennan et al., 2020; Van Deun et al., 2020; Sódar et al., 2016).

Anna D. Kashkanova and Martin Blessing contributed equally to this work.

Limitations in commonly used, label-free EV quantitation systems, such as nanoparticle tracking analysis (NTA), do not allow a distinction between EVs and co-isolated large LPs, resulting in inaccurate sizing and overestimation of EV numbers (Van Deun et al., 2020). Differential labelling of both populations is hindered by the fact that most pan-EV labelling methods rely on general lipophilic or protein-binding dyes, which will also label LPs (Botha et al., 2022). Measuring a separate lysis buffer control has been suggested to verify particle origin, for example when analysing EVs via flow cytometry, under the assumption that large LP particles would not be affected by this treatment (Welsh et al., 2020). Recently, however, this approach was shown to be inadequate (Botha et al., 2022).

Due to their different biochemical composition, EVs and large LPs differ in refractive index (RI). The RI is typically below 1.4 for EVs and above 1.4 for LPs (van der Pol et al., 2018). This results in distinct light-scattering properties, which can be used to separately analyse the two populations. However, until now this has only been successfully implemented for EVs larger than 200 nm, using a conventional flow cytometry-based approach (van der Pol et al., 2018). In another recent development, the different mechanical properties of EVs and lipoproteins have been used to discriminate them using atomic force microscopy (Ridolfi et al., 2022) This technique however has low throughput and the substrate can affect the particle properties. A sensitive method that allows label-free discrimination of EVs and large LPs in solution would be highly beneficial.

We have recently developed a novel particle detection technology called interferometric NTA (iNTA) (Kashkanova et al., 2022). The defining feature of iNTA is the use of interferometric detection of scattering (iSCAT), in which the light scattered by a particle is interfered with light reflected by a cover glass, leading to enhanced sensitivity for small particle sizes (Lindfors et al., 2004; Taylor & Sandoghdar, 2019). In addition, recording trajectories at high frame rates (5 kHz) and measuring the amount of scattered light allows for accurate estimation of both size and RI for each individual particle. Previously, we verified the sensitivity and reproducibility of this method for EV detection, and found that it was able to distinguish EVs from urinary protein complexes of similar size (Kashkanova et al., 2022). Here, we evaluated whether iNTA can be used to differentiate EVs from large LPs. Using mixtures of purified EVs and large LPs, as well as blood plasma samples purified by different methods, we show that iNTA can accurately measure the presence of bona fide EVs in plasma-derived samples of varying complexity.

2 | METHODS

2.1 | Lipoprotein stock solutions

Low-density and very-low-density lipoproteins were acquired from Sigma (437644 and 437647). Ultra-low-density lipoproteins (chylomicrons) were purchased from Lee Biosolutions (194-14).

2.2 | Cell culture and generation of conditioned medium

Melanoma cell line SKMEL37 was cultured in RPMI 1640 (Life Technologies) supplemented with 10% foetal bovine serum (FBS), 1% penicillin–streptomycin (Lonza) and 2 mM L-glutamine (Lonza). Cells were washed three times with serum-free medium and cultured in RPMI supplemented with 1% EV-depleted FBS for 24 h. FBS was depleted from EVs by ultracentrifugation (18 h, 100,000 × *g*). Conditioned medium (CM) (150 mL from ≈2E08 cells) was collected and centrifuged at 300 × *g* (10 min) and 2000 × *g* (20 min, 4°C). Next, CM was concentrated ≈300 times to 0.5 mL using a Centricon Plus-70 centrifugal filter device with a 10K nominal molecular weight limit (Merck Millipore).

2.3 | Blood collection

Venous blood was collected using a 21G needle in EDTA Vacutainers (BD367525, BD Biosciences). Pre-prandial blood of the healthy volunteer (male, 35 years old) was taken 12 h after the last meal. Post-prandial blood was collected 3 h after a meal with a caloric intake of ca. 1250 kCal (30% from fat). The melanoma patients included in this study (Figure 4: stage IB, female, 51 years old; Supp. Figure S17: stage IB, female, 57 years old) were not in a fasting state at the time of blood collection. Collection of blood samples was approved by the Ethical Committee of the FAU Erlangen-Nürnberg (registration number 496_20B) and was performed in accordance with relevant guidelines. Donors have given written informed consent.

2.4 | Plasma generation

Platelet-free plasma was prepared by two serial centrifugations at 2500 × *g* for 15 min, first at room temperature and then at 4°C. The supernatant was aliquoted and stored at −80°C. All samples were processed within 2 h after blood collection.

2.5 | Size-exclusion and dual-mode chromatography

SEC and DMC columns were prepared as described previously (Van Deun et al., 2020). Sepharose CL-4B (GE Healthcare) and Fractogel EMD SO_3^- (M) (Merck Millipore) resins were washed three times with PBS buffer. A nylon net with 20 μm pore size (NY2002500, Merck Millipore) was placed on the bottom of a 10 mL syringe (BD307736, BD Biosciences). For the SEC column, this was followed by stacking of 10 mL washed Sepharose. For the DMC column, 2 mL of Fractogel was stacked first, followed by careful layering of 10 mL Sepharose on top. After adding 0.5 mL plasma sample, the column was eluted by constant addition of fresh PBS. After discarding the void volume, which was 3 mL for SEC and 3.5 mL for DMC, 2 mL of EV-containing eluate was collected and concentrated to 100 μL using Amicon Ultra-2 10K filters (Merck Millipore).

2.6 | Density gradient

A discontinuous OptiPrep density gradient (DG) was constructed as described previously (Van Deun et al., 2014), with some modifications. Solutions of 5%, 10%, 20% and 40% iodixanol were made by mixing appropriate amounts of homogenization buffer (0.25 M sucrose, 1 mM EDTA, 10 mM Tris-HCL, pH 7.4) and OptiPrep stock solution (60% (w/v) aqueous iodixanol, Axis-Shield, Oslo, Norway). The gradient was formed by layering 3 mL of 40%, 3 mL of 20%, 3 mL of 10% and 2.5 mL of 5% solutions on top of each other in a 12 mL open top polyclear tube (Seton Scientific). 500 μL of sample was overlaid onto the top of the gradient, which was then centrifuged for 18 h at 100,000 × g and 4°C (TH641 rotor, Thermo Fisher). Afterwards, gradient fractions of 1 mL were collected from the top of the gradient and their density was estimated using a refractometer (Abbemat 200, Anton Paar). Fractions 7 and 8, corresponding to an EV density of 1.1–1.2 g/mL, were pooled and used for subsequent SEC-based separation of EVs from the iodixanol polymer, as described above and previously (Vergauwen et al., 2017). EV-containing fractions (F4-7) were pooled, concentrated to 100 μL, aliquoted into Protein LoBind tubes (Eppendorf), and stored at 4°C (maximum 48 h, for comparative NTA and iNTA measurements) or −80°C. For DG-based EV isolation of melanoma patient plasma, the gradient procedure described above was preceded by a SEC separation, based on Vergauwen et al. (2021). A total of 6 mL of plasma sample was divided over three SEC columns (2 mL of plasma per SEC column) followed by elution by PBS. Individual fractions of 1 mL were collected. Fraction 4–6 of three different columns were pooled and concentrated to 0.5 mL using an Amicon Ultra-15 10K filter (Merck Millipore). This was then placed on top of the gradient.

2.7 | Nanoparticle tracking analysis (NTA)

A Zetaview PMX-110 instrument, equipped with a 405 nm laser, was used to measure particle concentrations. Before sample measurement, the instrument was calibrated using 100 nm polystyrene beads diluted in water according to manufacturer's instructions. Cell temperature was maintained at 25°C for all measurements. Samples were diluted with PBS to be within a range of 50–250 particles per frame, in a total volume of 1 mL. Eleven cell positions were scanned for each measurement, using five cycles per position, with video recorded at 30 frames per second (total recorded video duration per sample was 55 s). Additional capture settings were: gain 719.52, shutter 50, minimum trace length 15. For measuring 40 nm and 60 nm PS beads, the gain was increased to 888.12. ZetaView software version 8.05.12 was used to analyse the recorded videos with the following settings: minimum brightness 25, maximum brightness 255, minimum area 5, and maximum area 200.

2.8 | Interferometric nanoparticle tracking analysis (iNTA)

An iNTA measurement setup (Kashkanova et al., 2022) was employed for the measurements. Measurements were done both in chambered cover glasses (IBIDI μ-Slide 18 well) and in home-made PVC chambers (Stein et al., 2017). The PVC chamber's bottom cover glasses were passivated with mPEG2000-Silane (Laysan Bio). For that purpose, borosilicate cover glasses (VWR) were sonicated in 2% Hellmanex III (Hellmanex Analytics) and milliQ (milliPore) subsequently for 10 min each. Clean cover glasses were dipped into ethanol and isopropanol before blow drying with nitrogen gas. The cover glasses were plasma cleaned (10 min in oxygen plasma at 500 W) and then incubated in 10 mg/mL mPEG2000-Silane at 50°C. mPEG200-Silane was dissolved in PEG reaction solution (95% Ethanol (v/v), 5% milliQ, pH was set to 2.0 with 1 M HCl). As soon as the buffer fully evaporated, cover glasses were sonicated for another 10 min in milliQ and blow dried with nitrogen gas. Passivated cover glasses were used the same day. The procedure for passivating the chambered cover glasses is similar, however the milliQ, ethanol and isopropanol cleaning steps were skipped.

For the measurement, the microscope focus was set at 1 μm above the cover glass. We have verified that the cover glass does not affect the size distribution by measuring particle size for various positions of the focal plane from 0 to 10 microns above the

cover glass (Figure S16). The field of view was 7.1 μm × 7.1 μm. Solutions were diluted, as to measure 1–7 trajectories with more than 100 localizations per second of recorded video. Videos of particles diffusing in 0.5–1.0 μL droplets of fluid on the cover glass (Figure S1) or in 50–100 μL volumes of fluid inside individual IBIDI wells were recorded for 10 min using pylablib cam-control (https://github.com/SandoghdarLab/pyLabLib-cam-control). To avoid evaporation, the used chambers were sealed. For small volumes (i.e. 0.5–1.0 μL), extra droplets of buffer were added adjacently. The additional liquid reservoir further reduced evaporation by saturating the humidity in the chamber (Figure S1). The records were analysed by applying median background correction and radial variance transform (Kashkanova et al., 2021). Particles were tracked using trackpy python package (Allan et al., 2021). Only trajectories with more than 100 localizations were kept. Particle size was extracted from its diffusion constant. The particle's scattering cross-section was extracted from its iSCAT contrast using previously performed calibration (Kashkanova et al., 2022). The effective RI was then calculated from the size and scattering cross-section.

To enable a direct comparison of particle concentrations measured by NTA and iNTA, we performed a calibration measurement using a dilution series of 60 nm polystyrene beads. This allowed us to extract a calibration factor for iNTA, which we used for converting a number of particle trajectories detected in a given time to a concentration in number of particles per mL (Figure S2).

2.9 | ELISA

Human Apolipoprotein B Quantikine ELISA Kit (R&D Systems, DAPB00) was used according to manufacturer's instructions. Standards and samples were assayed in duplicate. CD63 ELISA (Abcam, ab275099) was performed according to manufacturer's instructions. Due to limitations in available sample amount, samples were only assayed once.

2.10 | Western blotting

Equal volumes of EV samples were suspended in non-reducing sample buffer (0.05 M Tris–HCl (pH 6.8), 10% glycerol, 2% SDS, 1% bromophenol blue) and boiled for 5 min at 95°C. Proteins were separated by SDS-PAGE (SDS polyacrylamide gel electrophoresis), transferred to nitrocellulose membranes, blocked in 5% nonfat milk in PBS with 0.5% Tween-20, and immunostained overnight at 4°C using the following primary antibodies in a 1/1000 dilution in TBST: CD9 (BD555370), CD63 (BD556019), CD81 (BD555675). Blots were developed using the SuperSignal West Femto reagent (Thermo Fisher) and visualized on an Amersham 600 system (GE Healthcare). CD9 and CD81 were stained on the same membrane, which was stripped for 10 min using Restore Western blot stripping buffer (Life Technologies) in between staining.

2.11 | EV-TRACK knowledgebase

We have submitted all relevant data of our experiments to the EV-TRACK knowledgebase (EV-TRACK ID: EV220321). (Van Deun et al., 2017)

3 | RESULTS

3.1 | iNTA allows simultaneous size and refractive index estimation of EVs and large LPs

First, to compare the performance of NTA and iNTA for analysing biological nanoparticles, we measured the concentration and size of density gradient-purified cell culture EVs and commercial LP solutions. Given the interest in using EVs for cancer detection, the SKMEL37 melanoma cell line was selected as EV source. Measured particle concentrations for EVs and VLDLs were higher in iNTA compared to NTA, while for ULDLs they were similar (Table 1). We note that iNTA concentration measurements were calibrated using an NTA measurement of 60 nm polystyrene beads (see Methods and Figure S2) and are therefore not absolute. LDLs, a class of LPs which are typically smaller than EVs (<30 nm (Wojczynski et al., 2011)), were not detected accurately by NTA nor iNTA (Figure S3). Size distributions as measured by iNTA were narrower and shifted towards a smaller size, compared to NTA (Table 1 and Figure 1a). Indeed, using polystyrene spheres and silica beads of different sizes, we found that NTA generally returns a broader size distribution with an additional offset for small/weakly scattering particles (Figure S4), as was also shown previously by others (Arab et al., 2021; Bai et al., 2017; Usfoor et al., 2020). Taken together, these data show that iNTA has an increased sensitivity for smaller particles, whether artificial or biological, consistent with previous data (Kashkanova et al., 2022).

TABLE 1 Mean concentration and median size including interquartile range (IQR) of different classes of nanoparticles measured using NTA and iNTA. Refractive index (RI) is also shown for iNTA, calculated based on particles for which the simulated IQR (IQR_S) is smaller than 0.05 (see text). For concentration, the standard deviation of three successive measurements is indicated.

		NTA		iNTA		
		Mean concentration (particles/mL)	**Median size (IQR) (nm)**	**Mean concentration (particles/mL)**	**Median size (IQR) (nm)**	**Median RI (IQR) ($IQR_s < 0.05$)**
EVs	SKMEL37 cell culture-derived	6.7 ± 0.47 E11	126 (98-159)	1.58 ± 0.02 E12	97 (79–120)	1.37 (1.36–1.38)
Large LPs	Chylomicrons (ULDLs)	8.8 ± 0.39 E13	95 (76-120)	8.56 ± 0.57 E13	57 (48–71)	1.52 (1.48–1.57)
	Very low density lipoproteins (VLDLs)	1.8 ± 0.18 E12	76 (59-96)	2.80 ± 0.35 E13	46 (41–52)	1.49 (1.45–1.52)

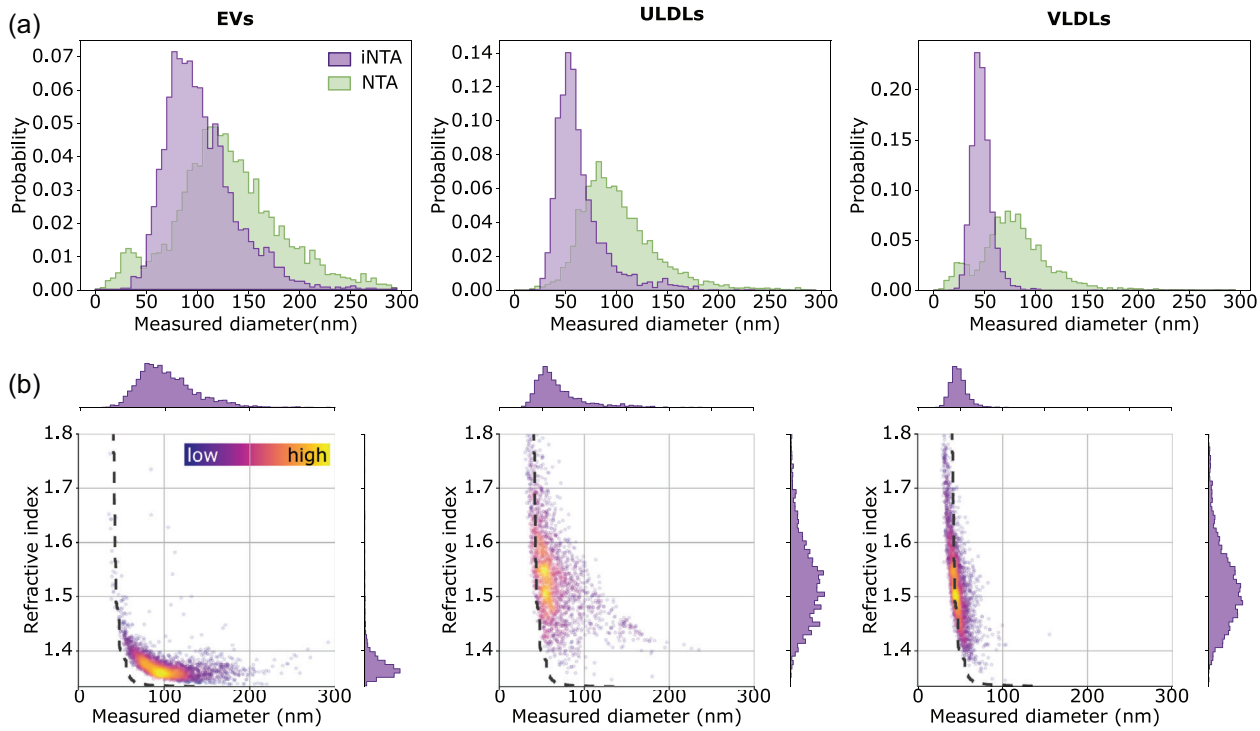

FIGURE 1 iNTA is more sensitive than NTA for smaller-sized EVs and LPs, and enables refractive index measurements. (a) EV, ULDL and VLDL size distributions as measured by NTA (green) and iNTA (purple). (b) Size-RI plots for EV, ULDL and VLDL measured by iNTA. Colour bar indicates the local density of points. In the region to the right of the dashed gray line, the IQR of RI based on simulations is smaller than 0.05.

Next, we aimed to differentiate EVs and large LPs based on their distinct light-scattering properties due to a difference in refractive index (RI) (van der Pol et al., 2018). We found that the mean scattering intensity of each particle as recorded by NTA could not be used to distinguish EVs from large LPs (Figure S5). For iNTA, however, the amount of light that is scattered by each particle is measured more precisely, using iSCAT contrast (Figure S4) (Kashkanova et al., 2022). This allowed us to plot size versus RI for EVs, ULDLs and VLDLs (Figure 1b). From these data, we noted a large spread in RI for smaller particle sizes, that is having a smaller iSCAT contrast. Measuring a suspension of immersion oil, with a nominal refractive index of 1.52, resulted in a similar spread (Figure S15). To estimate the precision with which iNTA can measure RI of particles of different sizes, we performed simulations to determine the interquartile range (simulated IQR or IQR_S) of RI arising exclusively due to measurement uncertainty in iSCAT contrast (Figure S15). To visualize this, the dashed lines in Figure 1b represent an IQR_S cutoff value of 0.05, with particles to the right of this line having a smaller IQR_S of the RI. Only considering those particles, we can derive distinct RIs for EVs (median RI of 1.37) and large LPs (median RIs of 1.52 for ULDLs and 1.49 for VLDLs) (Table 1). These values agree with those reported in literature (Chernova et al., 2018; Libregts et al., 2019).

Interestingly, aside from a small overlapping region of RI ≃ 1.4 and size 50–100 nm, EVs and large LPs appear as separate populations in the size-RI plots generated by iNTA. In order to separate the two populations, a refractive index cut-off could be used. However, choosing the value for this cut-off in an unbiased manner is non-trivial. Therefore, based on these measurements,

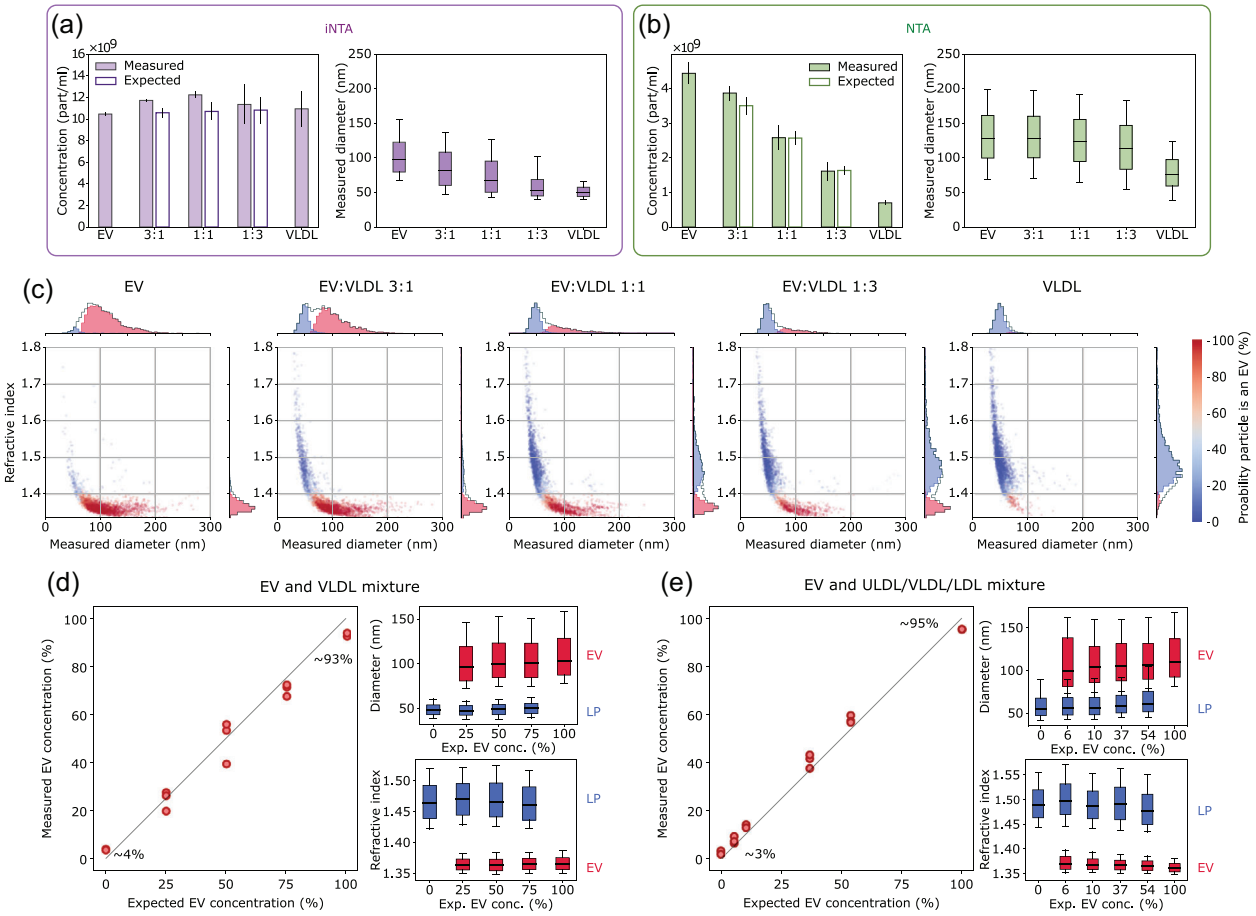

FIGURE 2 iNTA but not NTA can discriminate EVs and LPs in artificial mixtures. (a) iNTA and (b) NTA analysis of different EV-VLDL mixtures showing mean particle concentration (filled bars indicate the measured concentration while unfilled bars indicate the expected concentration based on measurements of pure EV and VLDL samples, standard deviation is shown) and median size (box boundaries are 25–75 percentile, horizontal line is median, whiskers indicate 10–90 percentile) ($n = 3$). Concentration for iNTA measurements is calculated by multiplying the number of trajectories measured in 10 min by a calibration factor determined previously (see Methods). (c) Representative size-RI plots for the different EV-VLDL mixtures, labelled using a random forest classifier. Colour indicates probability for the particle to be an EV. Only particles with greater than 80% probability of being an EV or less than 20% probability of being an LP are included in the 1D histograms. (d) Left: Measured relative EV concentration plotted versus expected relative EV concentration. The measured concentration is calculated as $C_{EV}/(C_{EV}+C_{VLDL})$, where C denotes particle concentration determined from plots in (c) using the random forest classifier. The numbers indicate the measured relative EV concentration when no EVs were expected (~4%) and when only EVs were expected (~93%). Right: The extracted diameter and refractive index of EVs (red) and lipoproteins (blue). RI was calculated by considering only particles with an $IQR_S < 0.05$. (e) Same as (d), but using a mixture of EVs with ULDLs, VLDLs and LDLs. Expected EV concentration was determined based on iNTA measurements of the pure EV sample and of the LP mixture.

a random forest classifier was constructed to discriminate EVs and LPs (Figure S6) (Breiman, 2001). For each particle with a given size, scattering cross-section and RI, the classifier returns the probability of it being an EV or a large LP. Using an 80% confidence threshold, iNTA measurements enable us to classify more than 85% of measured particles as either EVs or large LPs. This threshold was thus selected to be used in our further analyses.

3.2 | Mixed populations of EVs and LPs are discriminated by iNTA

Given the ability of iNTA to simultaneously determine RI and size for both EVs and LPs, we tested whether this would also allow accurate estimation of EV numbers in mixtures with LPs. We started with a mixture of SKMEL37 EVs with VLDLs in 3:1, 1:1 and 1:3 volume ratio. Roughly equal numbers of EVs and VLDLs as estimated by iNTA were chosen as starting material.

With iNTA, we measured equal total particle numbers for all mixtures, as expected (Figure 2a). The median size of the mixtures gradually decreased with increasing proportion of VLDLs, which were indeed measured to be almost two times smaller than EVs. NTA detected more than twofold fewer EVs and tenfold fewer VLDLs than iNTA (Figure 2b). As a result, a stepwise decrease in total particle concentration from EVs-only to VLDLs-only could be observed. However, even though VLDLs were measured to

be around 1.5 times smaller than EVs, the median size remained almost constant in all mixtures containing EVs. This confirms that NTA is biased towards larger particles which scatter more light (Arab et al., 2021), contributing to the fact that it could not distinguish between EVs and VLDLs in these mixtures (Figure S7). Even using iNTA, the broad size distributions of VLDLs and especially EVs did not allow for quantitative discrimination of the two particle types based on size alone. However, by simultaneously determining the RI for each particle, distinct populations could be resolved on size-RI plots using our machine learning classifier (Figure 2c, EVs indicated in red and LPs in blue). Indeed, this allowed us to reproduce the different ratios of EVs and VLDLs (Figure 2d—left panel). We were also able to extract size and RI of the individual EV and LP populations in the mixtures (Figure 2d—right panels). Technical replicates of these measurements showed only minor differences, demonstrating the robustness of iNTA for simultaneous size and RI determination of individual biological nanoparticles (Figure S8). To show that iNTA can also decipher more complex mixtures, we spiked four different quantities of EVs—spanning concentrations of 6% up to 54%—into a solution containing ULDLs, VLDLs and LDLs. Also in these samples, iNTA was able to accurately discriminate EVs from LPs (Figure 2e and Figure S9). The same mixtures measured by NTA again showed a good correspondence between observed and expected total particle concentrations, but no discrimination of the different particle types (Figure S10).

Summarizing the iNTA data, we found that 3%–4% of particles were misclassified as EVs in pure LP samples, while 5%–7% of particles were misclassified as LPs in pure EV samples. This demonstrates that iNTA, unlike NTA, is able to accurately detect genuine EVs in complex mixtures with LPs.

3.3 | iNTA enables bona fide EV quantification in plasma-derived samples

In order to evaluate the performance of iNTA to measure EVs in real-world samples, including the effect of variable plasma lipid composition, we collected blood plasma from a healthy volunteer in preprandial or postprandial state (i.e. before vs. 3 h after consuming a fatty meal). ELISA measurements confirmed an increase in the plasma concentration of ApoB, a marker for ULDLs, VLDLs and LDLs, after meal consumption (Figure S11). We also compared two EV enrichment methods, each known to remove LPs to a different extent. We used either size-exclusion chromatography (SEC), where all LPs with a similar size as EVs will be collected in the same fraction, or dual-mode chromatography (DMC), a method capable of removing >99% of ApoB-containing LPs (Van Deun et al., 2020).

As expected, ELISA measurements showed an increased ApoB concentration in post-versus preprandial EV samples, as well as in those obtained by SEC compared to DMC (Figure 3a). iNTA particle counts showed a similar result, increasing after meal consumption and SEC samples showing higher concentrations compared to DMC (Figure 3b). Similar trends in total particle concentrations were observed for conventional NTA (Figure S12). Extracting the nature of the particles from the size-RI plots generated by iNTA, we found that this increase in particle concentration is exclusively due to large LPs (Figure 3c). Indeed, the relative EV concentrations were below 4% for all unspiked samples (Figure 3d), consistent with the misclassification rate of LPs that we determined previously. The low level of EVs in samples from this particular individual was confirmed using a CD63 ELISA, with all measurements being below limit of detection (Figure S13).

To show that iNTA is able to accurately detect EVs in these samples, we decided to make use of an exogenous EV spike. The already purified SEC and DMC samples were spiked with cell culture EVs to obtain a theoretical EV concentration of 5E11 particles/mL and analysed by iNTA, as shown in Figure 3e,f. Despite the differences in LP background, iNTA was capable of extracting the spiked EV concentration from DMC and preprandial SEC samples with errors of less than 15% (Figure 3g). Due to high LP contamination in the postprandial SEC sample, its relative EV concentration was only marginally above the 4% misclassification rate and the error was close to 35% (Figure 3g). The same samples measured by NTA showed an increase in total particle concentration, however the spiked EV concentration could not be estimated (Figure S12). This demonstrates that EVs can be quantified by iNTA in plasma-derived samples of varying LP complexity, although the final accuracy will still depend on EV to LP ratio.

Finally, to show that iNTA is able to measure endogenous EVs derived from a lipid-rich sample, we collected plasma from a non-fasting melanoma patient. EV concentration was expected to be increased compared to healthy plasma, as shown previously for melanoma (Lee et al., 2019). EVs were isolated using SEC and DMC, as before, and also by a density gradient-based protocol (DG). This protocol is known to result in EVs of high purity (Vergauwen et al., 2021). A 12-times higher plasma sample input was used for the DG procedure as for SEC/DMC (6 mL vs. 0.5 mL). We could confirm the presence of EVs in all three samples using Western blotting for CD9, CD63 and CD81 (Figure 4a and Figure S14). The strongest signals were present in DG, as expected due to the higher sample input. To estimate the presence of LPs, we also measured ApoB concentration in these samples (Figure S11). The plasma sample was found to contain around 30% more ApoB than the postprandial healthy volunteer, indicating very high LP levels. SEC, DMC and DG each removed ApoB to a different extent, by around 25%, 99% and ˜100%, respectively. These same samples were then measured by iNTA. The SEC-processed sample contained a concentration of particles classified as EVs of 8.8E11 particles/mL, however with a relative concentration of only 3.7% due to high LP content, which is within the range of classification error (Figure 4b). DMC-based EV enrichment was not sufficient to avoid large LPs outnumbering EVs.

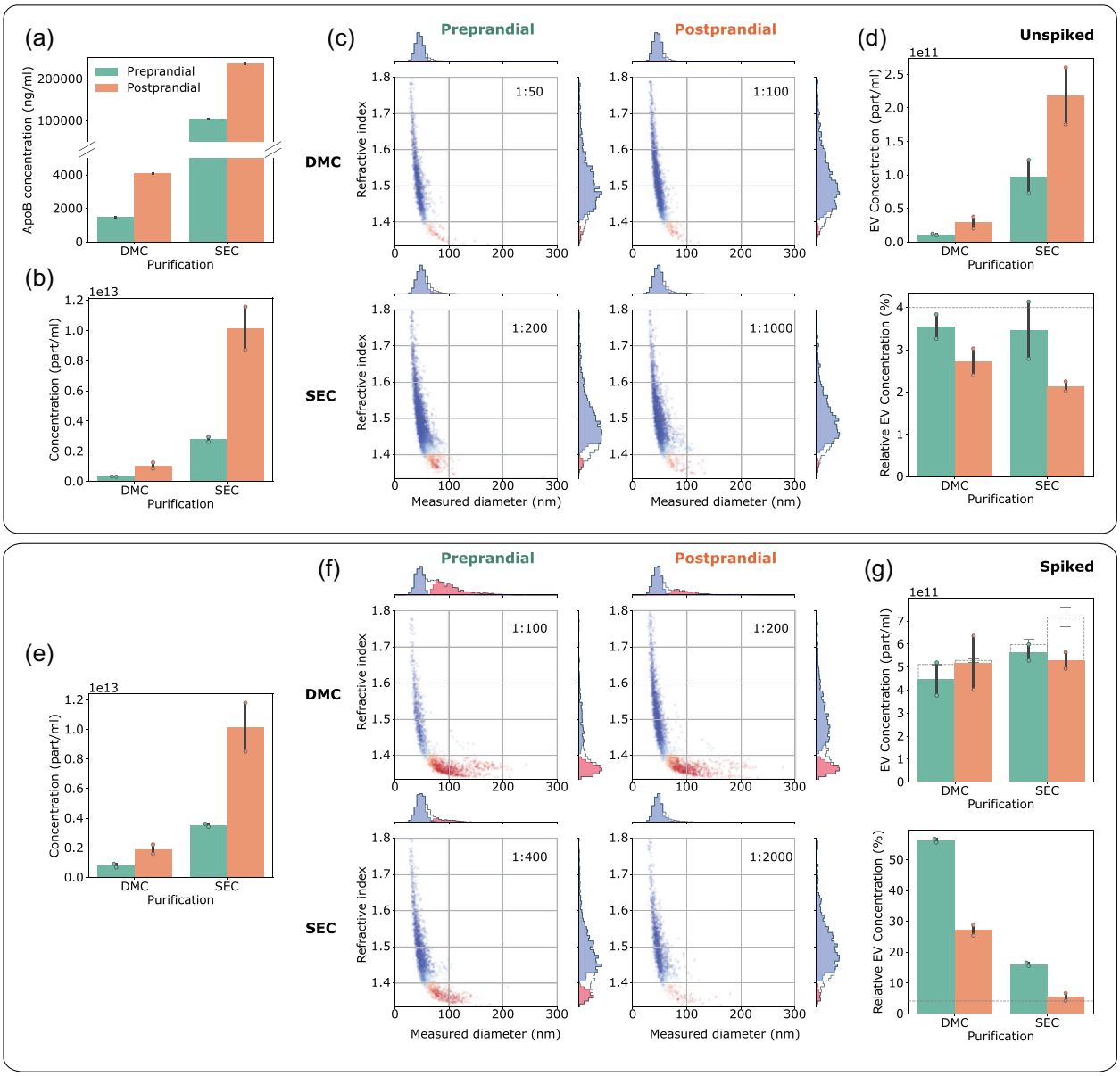

FIGURE 3 iNTA can accurately measure EVs in plasma-derived samples with variable LP background. (a) ApoB ELISA measurements in DMC- and SEC-processed samples (left and right), pre- and post-prandial (green and orange). (b) Total particle concentrations measured by iNTA. (c) Representative size-RI plots after machine learning processing (particles classified as EVs are indicated in red and LPs in blue). The numbers in the upper right corner indicate sample dilution factor by PBS prior to iNTA measurements. (d) EV concentration (top) and relative EV concentration (bottom) as determined by iNTA. Dashed line indicates the error threshold for EV classification (4%). (e)–(g) Same as (b)–(d) but for samples spiked with 5E11/mL SKMEL37 EVs. In (g) the dashed bars show the expected EV concentration based on values in (d). Mean and standard deviation are shown for all bar graphs ($n = 2$).

Nevertheless, iNTA could still identify a clear EV population with a concentration of 9.8E10 particles/mL and relative concentration of 7.2% (Figure 4c). For DG, iNTA detected a clear EV population with no background of large LPs (Figure 4d, EV concentration of 9.0E11 particles/mL and relative concentration of 97.7%). Interestingly, the DMC-purified sample appears to contain an EV population with slightly higher size and RI that is absent from the DG sample, which could be due to the association of EVs with the remaining HDL and LDL contaminants (see also Figure S17) (Busatto et al., 2020). Using these data and taking into account a previously-published recovery rate of 25% for the DG protocol (Geeurickx et al., 2019), the original EV concentration in this plasma sample was estimated to be around 6E10 particles/mL. The same calculation was made for the DMC and SEC measurements, using recovery rates of 33% and 80%, respectively (Van Deun et al., 2020). While the calculated value based on DMC agreed with that of ODG (5.9E10 particles/mL), SEC was off by a factor of four (2.2E11 particles/mL) due to the overwhelming presence of large LPs in this sample. This illustrates that iNTA can quantify EV populations even when outnumbered by large LPs by up to an order of magnitude.

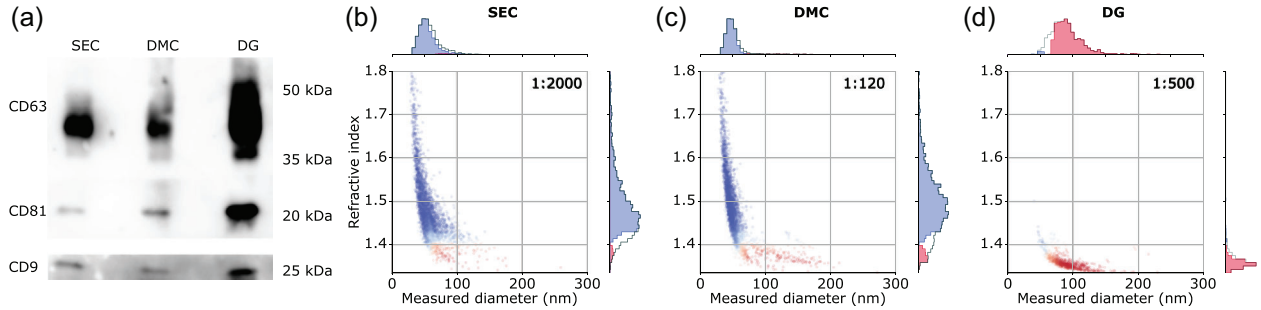

FIGURE 4 iNTA of EV samples enriched from lipemic melanoma patient plasma by SEC, DMC or DG. (a) Western blot of EV-associated tetraspanins. Equal volumes of EV sample were loaded, with DG (6 mL) having a 12× higher plasma sample input than SEC and DMC (0.5 mL). Size-RI plots of EVs enriched by (b) SEC; (c) DMC, arrowheads indicate the EV population; (d) DG. Numbers in the upper right corner indicate sample dilution factor by PBS prior to iNTA measurements.

4 | DISCUSSION

We have demonstrated that iNTA can discriminate EVs from large LPs in a label-free manner, through simultaneous determination of particle size and refractive index. We have constructed a machine learning classifier for EVs and large LPs, and experimentally validated that EV concentration can be quantified accurately, also when outnumbered by large LPs by up to an order of magnitude. iNTA measurements are highly sensitive, fast (recording up to 10,000 trajectories in 10 min), and require only a small sample volume ($\leq$1 μL). In addition, our work highlights the limited applicability of conventional NTA for determining EV concentration in complex mixtures of biological particles, such as blood plasma EV samples obtained by SEC. While total particle concentrations of EV-LP mixtures corresponded well to theoretical values, the relative contributions of EVs and LPs could not be determined by NTA. As large LPs outnumber EVs in many cases, NTA data have to be interpreted with care. Furthermore, conventional NTA does not reach a sufficient sensitivity towards smaller EVs (or LPs) in a heterogeneous population, whereas iNTA generally has a smaller size limit (~40 nm for biological nanoparticles).

Despite the clear advantages of iNTA, a few challenges remain. The reliance on RI to distinguish between EVs and LPs is inherently limited by their RI overlap. Especially for LPs, we found a broad RI distribution. While LPs are indeed reported to be highly heterogeneous (Packard & Shepherd, 1997), this is also due to technical factors. First, for smaller particles, the trajectories are shorter and therefore the error on particle size increases. Second, for particles with a small scattering cross-section, the relative error on iSCAT contrast is increased. Since RI is calculated from a combination of size and iSCAT contrast, the errors in both lead to a spread in RI. This also causes the narrowing of the RI distribution with increasing particle size, as seen in Figure S4. We conclude that, with the current data measurement and analysis settings, it is difficult to precisely determine RI of biological particles smaller than ~50 nm. As a result of these issues, about 6% of EVs are misclassified when using an 80% confidence threshold for our machine learning classifier. The accuracy of iNTA for EV quantification will therefore vary with the relative abundance of EVs and large LPs in a given sample. This limitation can be observed in the iNTA measurement of SEC EVs of the highly lipemic melanoma sample. While the number of particles classified as EVs was below the margin of error, Western blotting did identify similar EV marker presence as in the DMC sample.

Additional changes to iNTA could help to improve its performance further. In the current study, iNTA was implemented using static measurements inside nano/microliter droplets. Having a dynamic measurement, for example using a constant flow, would produce a more representative image of the sample. In addition, it could help to more accurately quantify lower numbers of EVs and cut down on measurement time. Another limitation concerns *absolute* concentration measurements. In this study, particle concentration measured by iNTA was calibrated using an NTA measurement of 60 nm PS beads. This strategy is suboptimal, given the known limitations of NTA for concentration measurements (Arab et al., 2021; Usfoor et al., 2020; Vestad et al., 2017). It is thus likely that the measured concentrations, for example for the melanoma patient, still do not represent the true number. A detailed study of independently using iNTA for absolute particle concentration determination is underway and will be reported elsewhere. Further possible improvements to iNTA include increasing the measurement sensitivity by using higher laser power and shorter wavelengths, improving data analysis to reduce the uncertainty in RI, adding measurements of zeta-potential on a single particle level to further improve differentiation between particle types, and expanding its capabilities for detecting labelled EV subpopulations by adding fluorescence filters. A significant advantage compared to current single particle fluorescence approaches would be that mislabelled non-EV particles can be filtered out using RI measurements.

Overall, iNTA outperformed conventional NTA. Indeed, we envision it could have a broad impact on EV research as a new standard for label-free EV sizing and quantification. It could also facilitate the translational application of EVs, for example by improving EV-based biomarker normalization and enabling superior quality control of EV products such as reference materials and therapeutics.

AUTHOR CONTRIBUTIONS

Anna D. Kashkanova: Conceptualization; data curation; formal analysis; investigation; methodology; resources; software; visualization; writing—original draft; writing—review and editing. **Martin Blessing**: Conceptualization; data curation; formal analysis; investigation; methodology; resources; software; writing—review and editing. **Marie Reischke**: Investigation; writing—review and editing. **Jan-Ole Baur**: Investigation; writing—review & editing. **Andreas S. Baur**: Funding acquisition; supervision; writing—review & editing. **Vahid Sandoghdar**: Funding acquisition; supervision; writing—review and editing. **Jan Van Deun**: Conceptualization; data curation; formal analysis; investigation; methodology; resources; writing—original draft; writing—review and editing.

ACKNOWLEDGEMENTS

We thank the Max Planck Society and the Bundesministerium für Bildung und Forschung for financial support. A.D.K. was supported by a Christiane Nüsslein-Volhard-Stiftung Fellowship and Alexander von Humboldt-Stiftung Postdoctoral Fellowship.

CONFLICT OF INTEREST STATEMENT

A.D.K., M.B., and V.S. have filed an International Patent Application (PCT) based on this work in the name of the Max Planck Gesellschaft zur Förderung der Wissenschaften e.V. J.V.D. is listed as co-inventor on a patent concerning dual-mode chromatography (US20230070693). The other authors declare no conflicts of interest.

DATA AVAILABILITY STATEMENT

The data that support the findings of this study are available from the corresponding authors upon request.

REFERENCES

Allan, D. B., Caswell, T., Keim, N. C., van der Wel, C. M., & Verweij, R. W. (2021). soft-matter/trackpy: Trackpy v0.5.0.

Arab, T., Mallick, E. R., Huang, Y., Dong, L., Liao, Z., Zhao, Z., Gololobova, O., Smith, B., Haughey, N. J., Pienta, K. J., Slusher, B. S., Tarwater, P. M., Tosar, J. P., Zivkovic, A. M., Vreeland, W. N., Paulaitis, M. E., & Witwer, K. W. (2021). Characterization of extracellular vesicles and synthetic nanoparticles with four orthogonal single-particle analysis platforms. *Journal of Extracellular Vesicles*, *10*(6), e12079.

Bai, K., Barnett, G. V., Kar, S. R., & Das, T. K. (2017). Interference from proteins and surfactants on particle size distributions measured by nanoparticle tracking analysis (NTA). *Pharmaceutical Research*, *34*, 800–808.

Botha, J., Handberg, A., & Simonsen, J. B. (2022). Lipid-based strategies used to identify extracellular vesicles in flow cytometry can be confounded by lipoproteins: Evaluations of annexin V, lactadherin, and detergent lysis. *Journal of Extracellular Vesicles*, *11*(4), e12200.

Breiman, L. (2001). Mach. *Learn*, *45*, 5–32.

Brennan, K., Martin, K., FitzGerald, S. P., Wu, Y., Blanco, A., Richardson, C., & Mc Gee, M. M. (2020). A comparison of methods for the isolation and separation of extracellular vesicles from protein and lipid particles in human serum. *Scientific Reports*, *10*(1), 1–13.

Busatto, S., Yang, Y., Walker, S. A., Davidovich, I., Lin, W. H., Lewis-Tuffin, L., Anastasiadis, P. Z., Sarkaria, J., Talmon, Y., Wurtz, G., & Wolfram, J. (2020). Brain metastases-derived extracellular vesicles induce binding and aggregation of low-density lipoprotein. *Journal of Nanbiotechnology*, *18*, 162.

Chernova, D. N., Konokhova, A. I., Novikova, O. A., Yurkin, M. A., Strokotov, D. I., Karpenko, A. A., Chernyshev, A. V., & Maltsev, V. P. (2018). Chylomicrons against light scattering: The battle for characterization. *Journal of Biophotonics*, *11*(10), e201700381.

Van Deun, J., Jo, A., Li, H., Lin, Y., Weissleder, R., Im, H., & Lee, H. (2020). Integrated dual-mode chromatography to enrich extracellular vesicles from plasma. *Advanced Biosystems*, *4*(12), 1900310.

Van Deun, J., Mestdagh, P., Sormunen, R., Cocquyt, V., Vermaelen, K., Vandesompele, J., Bracke, M., Wever, O. D., & Hendrix, A. (2014). The impact of disparate isolation methods for extracellular vesicles on downstream RNA profiling. *Journal of Extracellular Vesicles*, *3*, 24858.

Geeurickx, E., Tulkens, J., Dhondt, B., Van Deun, J., Lippens, L., Vergauwen, G., Heyrman, E., De Sutter, D., Gevaert, K., Impens, F., Miinalainen, I., Van Bockstal, P., De Beer, T., Wauben, M. H. M., Nolte-t-Hoen, E. N., Bloch, K., Swinnen, J. V., Nieuwland, R., Braems, G., … Hendrix, A. (2019). The generation and use of recombinant extracellular vesicles as biological reference material. *Nature Communications*, *10*(1), 1–12.

Kashkanova, A. D., Blessing, M., Gemeinhardt, A., Soulat, D., & Sandoghdar, V. (2022). Precision size and refractive index analysis of weakly scattering nanoparticles in polydispersions. *Nature Methods*, *19*, 586–593.

Kashkanova, A. D., Shkarin, A. B., Mahmoodabadi, R. G., Blessing, M., Tuna, Y., Gemeinhardt, A., & Sandoghdar, V. (2021). Precision single-particle localization using radial variance transform. *Optics Express*, *29*, 11070–11083.

Lee, H., Dindorf, J., Eberhardt, M., Lai, X., Ostalecki, C., Koliha, N., Gross, S., Blume, K., Bruns, H., Wild, S., Schuler, G., Vera, J., & Baur, A. S. (2019). Innate extracellular vesicles from melanoma patients suppress β-catenin in tumor cells by miRNA-34a. *Life Science Alliance*, *2*(2), e201800205.

Libregts, W. M., Rikkert, L. G., Hau, C. M., Nieuwland, R., & Coumans, A. W. (2019). Refractive index to evaluate staining specificity of extracellular vesicles by flow cytometry. *Journal of Extracellular Vesicles*, *8*(1), 1643671.

Lindfors, K., Kalkbrenner, T., Stoller, P., & Sandoghdar, V. (2004). Detection and spectroscopy of gold nanoparticles using supercontinuum white light confocal microscopy. *Physical Review Letters*, *93*(3), 037401.

Packard, C. J., & Shepherd, J. (1997). Lipoprotein heterogeneity and apolipoprotein b metabolism. *Arteriosclerosis, Thrombosis, and Vascular Biology*, *17*, 3542–3556.

Ridolfi, A., Conti, L., Brucale, M., Frigerio, R., Cardellini, J., Musicò, A., Romano, M., Zendrini, A., Polito, L., Bergamaschi, G., Gori, A., Montis, C., Barile, L., Berti, D., Radeghieri, A., Bergese, P., Cretich, M., & Valle, F. (2022). Compositional profiling of EV-lipoprotein mixtures by AFM nanomechanical imaging. *BioRxiv, 2022.07.19.500441*. Compositional profiling of EV-lipoprotein mixtures by AFM nanomechanical imaging.

Simonsen, J. B. (2017). What are we looking at? extracellular vesicles, lipoproteins, or both? *Circulation Research*, *121*, 920–922.

Sódar, B. W., Kittel, Á., Pálóczi, K., Vukman, K. V., Osteikoetxea, X., Szabó-Taylor, K., Németh, A., Sperlágh, B., Baranyai, T., Giricz, Z., Wiener, Z., Turiák, L., Drahos, L., Pállinger, É., Vékey, K., Ferdinandy, P., Falus, A., & Buzás, E. I. (2016). Low-density lipoprotein mimics blood plasma-derived exosomes and microvesicles during isolation and detection. *Scientific Reports*, *6*, 24316.

Stein, H., Spindler, S., Bonakdar, N., Wang, C., & Sandoghdar, V. (2017). Production of isolated giant unilamellar vesicles under high salt concentrations. *Frontiers in Physiology*, *8*, 63.

Taylor, R. W., & Sandoghdar, V. (2019). Interferometric scattering microscopy: Seeing single nanoparticles and molecules via rayleigh scattering. *Nano Letters*, *19*, 4827–4835.

Usfoor, Z., Kaufmann, K., Rakib, A. S. H., Hergenroder, R., & Shpacovitch, V. (2020). Features of sizing and enumeration of silica and¨ polystyrene nanoparticles by nanoparticle tracking analysis (NTA). *Sensors*, *20*, 6611.

van der Pol, E., de Rond, L., Coumans, F. A., Gool, E. L., Böing, A. N., Sturk, A., Nieuwland, R., & van Leeuwen, T. G. (2018). Absolute sizing and label-free identification of extracellular vesicles by flow cytometry. *Nanomedicine: Nanotechnology, Biology and Medicine*, *14*(3), 801–810.

Van Deun, J., Mestdagh, P., Agostinis, P., Akay, Ö., Anand, S., Anckaert, J., Martinez, Z. A., Baetens, T., Beghein, E., Bertier, L., Berx, G., Boere, J., Boukouris, S., Bremer, M., Buschmann, D., Byrd, J. B., Casert, C., Cheng, L., Cmoch, A., … Hendrix, A. (2017). EV-TRACK: Transparent reporting and centralizing knowledge in extracellular vesicle research. *Nature Methods*, *14*(3), 228–232.

Vergauwen, G., Dhondt, B., Van Deun, J., De Smedt, E., Berx, G., Timmerman, E., Gevaert, K., Miinalainen, I., Cocquyt, V., Braems, G., Denys, H., De Wever, O., & Hendrix, A. (2017). Confounding factors of ultrafiltration and protein analysis in extracellular vesicle research. *Scientific Reports*, *7*(1), 1–12.

Vergauwen, G., Tulkens, J., Pinheiro, C., Cobos, F. A., Dedeyne, S., Scheerder, A. D., Vandekerckhove, L., Impens, F., Miinalainen, I., Braems, G., Gevaert, K., Mestdagh, P., Vandesompele, J., Denys, H., Wever, O. D., & Hendrix, A. (2021). Robust sequential biophysical fractionation of blood plasma to study variations in the biomolecular landscape of systemically circulating extracellular vesicles across clinical conditions. *Journal of Extracellular Vesicles*, *10*(10), e12122.

Vestad, B., Llorente, A., Neurauter, A., Phuyal, S., Kierulf, B., Kierulf, P., Skotland, T., Sandvig, K. F., Haug, K. B., & Øvstebø, R. (2017). Size and concentration analyses of extracellular vesicles by nanoparticle tracking analysis: A variation study. *Journal of Extracellular Vesicles*, *6*(1), 1344087.

Welsh, J. A., Der Pol, E. V., Arkesteijn, J. A., Bremer, M., Brisson, A., Coumans, F., Dignat-George, F., Duggan, E., Ghiran, I., Giebel, B., Görgens, A., Hendrix, A., Lacroix, R., Lannigan, J., Libregts, W. M., Lozano-Andrés, E., Morales-Kastresana, A., Robert, S., Rond, L. D., … Jones, J. C. (2020). MIFlowCyt-EV: A framework for standardized reporting of extracellular vesicle flow cytometry experiments. *Journal of Extracellular Vesicles*, *9*(1), 1713526.

Wojczynski, M. K., Glasser, S. P., Oberman, A., Kabagambe, E. K., Hopkins, P. N., Tsai, M. Y., Straka, R. J., Ordovas, J. M., & Arnett, D. K. (2011). High-fat meal effect on LDL, HDL, and VLDL particle size and number in the genetics of lipid-lowering drugs and diet network (GOLDN): An interventional study. *Lipids in Health and Disease*, *10*, 181.

SUPPORTING INFORMATION

Additional supporting information can be found online in the Supporting Information section at the end of this article.

How to cite this article: Kashkanova, A. D., Blessing, M., Reischke, M., Baur, J.-O., Baur, A. S., Sandoghdar, V., & Van Deun, J. (2023). Label-free discrimination of extracellular vesicles from large lipoproteins. *Journal of Extracellular Vesicles*, *12,* e12346. https://doi.org/10.1002/jev2.12348